Architecture and Control Algorithms for Combating Partial Shading in Photovoltaic Systems

Yanzhi Wang, *Student Member*, *IEEE*, Xue Lin, *Student Member*, *IEEE*, Younghyun Kim, *Member*, *IEEE*, Naehyuck Chang, *Fellow*, *IEEE* and Massoud Pedram, *Fellow*, *IEEE*

***Abstract*—Partial shading is a serious obstacle to the effective utilization of photovoltaic (PV) systems since it can result in a significant degradation in the PV system output power. A PV system is organized as a series connection of PV modules, each module comprising a number of series-parallel connected PV cells. Backup PV cell employment and PV module reconfiguration techniques have been proposed to improve the performance of the PV system under the partial shading effects. These approaches are however not very effective since they are costly in terms of their PV cell count and/or cell connectivity requirements. In contrast, this paper presents a cost-effective, reconfigurable PV module architecture with integrated switches in each PV cell. The paper also presents a dynamic programming algorithm to adaptively produce near-optimal reconfigurations of each PV module so as to maximize the PV system output power under any partial shading pattern. We implement a working prototype of reconfigurable PV module with 16 PV cells and confirm 45.2% output power level improvement. Using accurate PV cell models extracted from prototype measurement, we have demonstrated up to a factor of 2.36X output power improvement of a large-scale PV system comprised of 3 PV modules with 60 PV cells per module.**

***Index Terms*—Photovoltaic system, partial shading, photovoltaic module reconfiguration, dynamic programming.**

I. Introduction

DUE to an increasing appetite for energy sources and environmental concerns about fossil fuels, there has been a growing demand for renewable energy resources (e.g., solar, wind, geothermal), which are clean and eco-friendly. The energy produced from renewable energy resources must be cost-competitive with the energy produced from fossil fuels. Photovoltaic (PV) energy generation techniques have received significant attention since they utilize the abundance of solar energy and can easily be scaled up. Thanks to extensive research and development of PV energy generation technologies, various scales of PV energy generation systems (PV systems) have been deployed for many practical applications such as PV power stations, solar-powered vehicles, and solar-powered heating and lighting appliances.

Fig. 1 shows the PV system architecture considered in this paper. Several PV modules are connected in series to provide a desirable output voltage level. We call such series-connected PV modules a *PV* (*module*) *string*. In the conventional realization of a PV system, each PV module consists of $n \times m$ PV cells connected in series/parallel i.e., each PV module has a fixed configuration.

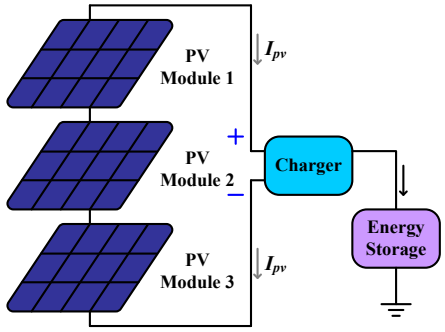

Fig. 1. The PV system architecture based on the string charger architecture.

The PV string is then fed to a charger, which regulates the operation of PV modules with the help of appropriate control circuitry. This PV system architecture reduces the hardware cost due to sharing of the charger among different PV modules. We call such a PV system architecture the *string charger architecture*. An electrical energy storage (EES) system is connected to the charger to store the electrical energy harvested by the PV modules.

The PV system output power level, i.e., the output power of the charger in the PV system, depends on the solar irradiance, which is changing frequently according to the time of day and weather conditions. The PV cells exhibit highly non-linear voltage-current (V-I) output characteristics (curves) that change with the solar irradiance level. Fig. 2 (a) shows the PV cell V-I output characteristics under different solar irradiance levels. Fig. 2 (b) shows the corresponding voltage-power (V-P) output characteristics. The red dots in Fig. 2 denote the *maximum power points* (MPPs) of a PV cell where the PV cell achieves the maximum output power for the given solar irradiance level. Ideally, all PV cells in the PV system experience the same solar irradiance level and thus exhibit the

This research is sponsored in part by grants from the Software and Hardware Foundations of the Division of Computer and Communication Foundations of the U.S. National Science Foundation, the Brain Korea 21 Project, the National Research Foundation of Korea (NRF) grant funded by the Korean Government (MEST) (No. 20120005640). The SPORT lab at USC and the ICT at Seoul National University provide research facilities for this study.

Y. Wang, X. Lin, and M. Pedram are with the Department of Electrical Engineering, University of Southern California, Los Angeles, CA, USA (email: yanzhiwa@usc.edu, xuelin@usc.edu, pedram@usc.edu).

Y. Kim is with the School of Electrical and Computer Engineering, Purdue University, West Lafayette, IN, USA (email: yhkim1@purdue.edu).

N. Chang is with the Department of Electrical Engineering and Computer Science, Seoul National University, Seoul, South Korea (e-mail: naehyuck@elpl.snu.ac.kr).

N. Chang and M. Pedram are co-corresponding authors.

same V-I and V-P output characteristics. Consequently, all the PV cells can simultaneously operate at their MPPs, and the PV string achieves the maximum output power since the output voltage of the PV string is set to be a desired value by the charger. Usually, a *maximum power point tracking* (MPPT) technique is implemented in the control circuitry of the PV system to find the desired output voltage for the PV string, where the PV string can achieve the maximum output power [2], [3]. It has recently been shown that the *maximum power transfer tracking* (MPTT) method, which accounts for the variation in the conversion efficiency of the charger as a function of the output power of the PV string and the state of charge of the EES elements, can be even more effective than the MPPT methods [4], [5], [6].

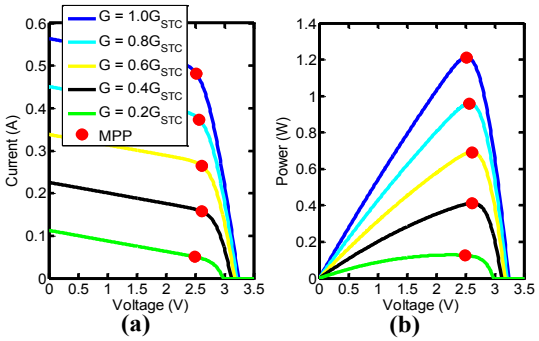

Fig. 2. PV cell (a) V-I and (b) V-P output characteristics under different solar irradiance level G. The red dots denote MPPs of a PV cell, where the PV cell achieves the maximum output power under certain solar irradiance level.

In reality, the solar irradiance levels received by PV cells in a PV system may be different from each other when a portion of PV modules is in shadow, and such a phenomenon is known as the *partial shading* effect. For example, moving clouds cause partial shading for stationary applications. On the other hand, shadows from nearby objects (e.g., buildings, trees, and poles) produce partial shading for PV systems on hybrid electric vehicles, which is much more severe as vehicles are moving through shaded or lighted regions.

PV cells generally have different MPPs under the partial shading effect. Partial shading not only reduces the maximum output power of the shaded PV cells, but also makes the lighted or less-shaded PV cells that are connected in series with the shaded ones to deviate from their MPPs. In other words, the PV cells cannot simultaneously operate at their MPPs. The PV systems with the string charger architecture are extremely vulnerable to partial shading since the PV modules are connected in series. With partial shading, the maximum output power of a PV string becomes much lower than the sum of the maximum output power values of all the individual PV cells in the PV string. In addition, partial shading may result in multiple power peaks in the V-P output characteristics of a PV string. Therefore, the MPPT (or MPTT) techniques must be modified in order to dynamically track a global optimum operating point instead of a local optimal one [7], [8], [9], [10]. This is because the existing MPPT or MPTT techniques such as the *perturb and observe* method rely on the unimodality assumption about the V-P output characteristics of the PV string. The modified MPPT or MPTT techniques increase the complexity of the PV system control circuitry.

The modified MPPT techniques may restore part of the power loss due to partial shading, but they cannot fully utilize the lighted PV cells due to the deviation from their MPPs caused by the shaded cells. On the other hand, PV module reconfiguration techniques, which have the potential of fully exploiting the MPPs of both lighted and shaded PV cells in a partially shaded PV string, can help maintain the output power level of a PV system under partial shading. Various PV reconfiguration techniques have been proposed, which are different from each other in terms of the system structure and control approach [11], [12], [13], [14], [15]. However, they suffer from one or more of the following limitations:

1) To compensate the power loss from shaded PV cells, many extra PV cells are needed for performing reconfiguration according to the shading pattern;
2) There is a lack of systematic and scalable structural support or effective control mechanism;
3) Variations in the conversion efficiency of the charger or inverter at different operating points are overlooked, which may result in a sizeable degradation in the overall energy conversion efficiency;
4) The PV system employs an *individual charger architecture*, in which each PV module has an individual charger for setting the operating point, thereby increasing the hardware cost of the PV system. A more widely used and cost-effective structure is the string charger architecture.

In this paper, we present a PV module reconfiguration approach that provides both a scalable reconfiguration architecture as well as a systematic and near-optimal control mechanism to overcome the PV system output power degradation caused by partial shading. The PV module reconfiguration controller dynamically updates the PV module configurations according to the changing partial shading pattern and conversion efficiency variation of the charger. We employ a reconfigurable PV module architecture, which was first introduced in reference [16] to realize the balanced reconfiguration of supercapacitor banks in hybrid EES (HEES) systems. This reconfigurable PV module architecture can also be applied for PV systems in hybrid electric vehicles [17] and PV systems online fault detection and tolerance [18]. We use the reconfigurable PV module architecture to realize flexible PV module configurations, in which there can be an arbitrary number of *PV groups* connected in series. Note that a PV group consists of parallel-connected PV cells where the number of PV cells in each PV group can be different from each other.

We also develop an effective reconfiguration control mechanism for PV systems with the string charger architecture. We focus on the string charger architecture since it is widely used and more cost effective than other architectures. Our reconfiguration control mechanism adaptively finds the near-optimal PV module configuration for each PV module according to the partial shading pattern and the conversion efficiency variation of the charger such that both the shaded and lighted PV cells can work at or close to their MPPs simultaneously. In this way, we improve the PV system output power level under partial shading conditions to the largest possible extent. The proposed reconfiguration control mechanism is based on a dynamic programming algorithm with polynomial time complexity, and therefore, it can be incorporated into modern PV systems with negligible extra computational overhead. We implement a working prototype of

reconfigurable PV module with 16 PV cells and confirm 45.2% output power level improvement. Using accurate PV cell modules extracted from prototype measurement, we have demonstrated up to a factor of 2.36X output power improvement of a large-scale PV system comprised of 3 PV modules with 60 PV cells per modules.

II. Component Models

A. PV Cell Model and Characterization

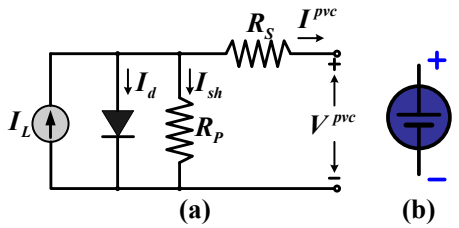

Fig. 3. The equivalent circuit model (a) and the symbol (b) of a PV cell.

Every PV module consists of multiple PV cells. Let V^{pvc} and I^{pvc} denote the output voltage and current of a PV cell, respectively. The PV cell equivalent circuit model is shown in Fig. 3 (a) with the V-I output characteristics given by

$$\begin{aligned} I^{pvc} &= I_L - I_d - I_{sh} \\ &= I_L(G) - I_0(T)\left(e^{(V^{pvc}+I^{pvc}\cdot R_s)\cdot\frac{q}{AkT}} - 1\right) \\ &\quad - \frac{V^{pvc}+I^{pvc}\cdot R_s}{R_p}, \end{aligned} \tag{1}$$

where

$$I_L(G) = \frac{G}{G_{STC}} \cdot I_L(G_{STC}), \tag{2}$$

and

$$I_0(T) = I_0(T_{STC}) \cdot \left(\frac{T}{T_{STC}}\right)^3 \cdot e^{\frac{qE_g}{Ak}\cdot\left(\frac{1}{T_{STC}} - \frac{1}{T}\right)}. \tag{3}$$

Parameters in (1) – (3) are defined as follows. G is the solar irradiance level; T is the cell temperature; q is the charge of the electron; E_g is the energy bandgap; and k is the Boltzmann's constant. STC stands for *standard test condition* in which the irradiance level is 1000 W/m^2 and the cell temperature is 25 °C. We adopt the method proposed in [19] to extract the unknown parameter values from the measured PV cell's V-I curve at any specific environmental condition $(G,\ T)$. These parameters include the following: the photo-generated current at STC $I_L(G_{STC})$, dark saturation current at STC $I_0(T_{STC})$, PV cell series resistance R_s, PV cell parallel (shunt) resistance R_p, and diode ideality factor A. We obtain the V-I output characteristics of a PV cell of given environmental conditions $(G,\ T)$ based on this PV cell model.

B. Charger Model

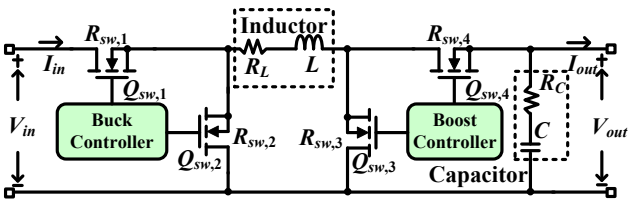

Fig. 4. The architecture of buck-boost switching converter.

Fig. 4 shows the model of a PWM (pulse width modulation) buck-boost switching converter, which is used as the charger in the proposed PV system. The input ports of the charger are connected to the PV string, whereas the output ports are connected to the EES element. The charger regulates the operating point of the PV string by controlling the charger's input voltage, i.e., the PV output voltage (and then the PV string output current is automatically determined by its V-I characteristics.) We denote the input voltage, input current, output voltage and output current of the charger by V_{in}, I_{in}, V_{out}, and I_{out}, respectively. According to the energy conservation law, the power loss of the charger P_{conv} satisfies the following identity:

$$V_{in} \cdot I_{in} = P_{conv} + V_{out} \cdot I_{out}. \tag{4}$$

Depending on the relationship between V_{in} and V_{out}, the charger operates in one of the two possible operating modes: the buck mode when $V_{in} > V_{out}$ and the boost mode otherwise [20], [21]. When the charger is operating in the buck mode, its power loss P_{conv} is given by

$$\begin{aligned} P_{conv} &= I_{out}^2 \cdot (R_L + D\cdot R_{sw,1} + (1-D)\cdot R_{sw,2} + R_{sw,4}) \\ &+ \frac{(\Delta I)^2}{12}\cdot\left(R_L + D\cdot R_{sw,1} + (1-D)\cdot R_{sw,2} + R_{sw,4} + R_C\right) \\ &+ V_{in}\cdot f_s\cdot\left(Q_{sw,1} + Q_{sw,2}\right) + V_{in}\cdot I_{controller}, \end{aligned} \tag{5}$$

where $D = V_{out}/V_{in}$ is the PWM duty ratio and $\Delta I = V_{out}\cdot(1-D)/(L\cdot f_s)$ is the maximum current ripple; f_s is the switching frequency; $I_{controller}$ is the current of the micro-controller of the charger; R_L and R_C are the internal series resistances of the inductor L and the capacitor C, respectively; $R_{sw,i}$ and $Q_{sw,i}$ are the turn-on resistance and gate charge of the i^{th} MOSFET switch shown in Fig. 4, respectively.

The charger power loss P_{conv} in the boost mode is given by

$$\begin{aligned} P_{conv} &= \left(\frac{I_{out}}{1-D}\right)^2 \cdot \\ &(R_L + D\cdot R_{sw,3} + (1-D)R_{sw,4} + R_{sw,1} + D(1-D)R_C) \\ &+ \frac{(\Delta I)^2}{12}(R_L + DR_{sw,3} + (1-D)\left(R_{sw,4} + R_C\right) + R_{sw,1}) \\ &+ V_{out}\cdot f_s\cdot\left(Q_{sw,3} + Q_{sw,4}\right) + V_{in}\cdot I_{controller}, \end{aligned} \tag{6}$$

where $D = 1 - V_{in}/V_{out}$ and $\Delta I = V_{in}\cdot D/(L\cdot f_s)$.

The power dissipation of the charger is minimized when (i) the input voltage and the output voltage of the charger are close to each other and (ii) the output current of the charger is within a certain range. Let $I_{out} = Chg\_Out\_I(V_{in}, I_{in}, V_{out})$ denote the function that calculates I_{out} based on V_{in}, I_{in}, and V_{out}.

III. Partial Shading Effect

We demonstrate that the partial shading effect may significantly degrade the output power level of a PV module with a fixed $n \times m$ configuration. We use a PV module with a 2×2 configuration as an example. As shown in Fig. 5, the PV module consists of two series-connected PV groups, and each PV group consists of two parallel-connected PV cells. The PV cell at the bottom right is completely shaded (with no solar irradiance) while the rest of PV cells receive the solar irradiance under the standard test condition i.e., $G_{STC} = 1000$ W/m^2. Since only one PV cell out of four is shaded, the

ideal setup should exhibit the PV module output power degradation of 25% compared to the same PV module without any shading. However, the actual PV module output power degradation is much larger than 25%.

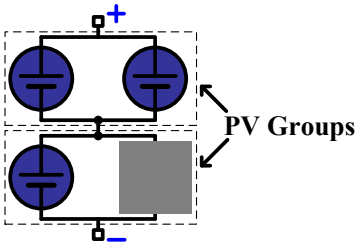

Fig. 5. A 2 × 2 PV module with one PV cell completely shaded.

We plot in Fig. 6 the V-I characteristics of the PV module under partial shading. Curve 1 corresponds to the V-I output characteristics of the bottom PV group with the shaded PV cell, whereas Curve 2 corresponds to the V-I output characteristics of the top PV group. Curve 2 has a higher current value than Curve 1 at the same voltage value. Curve 3 is the V-I output characteristics of the PV module, which is directly derived from Curves 1 and 2 since PV module is a series connection of the two PV groups. We assume that each PV cell is integrated with a bypass diode to protect the PV cell from reverse bias operation under partial shading [22] when we derive Curve 3.

We compare the end-to-end V-P output characteristics of the partially shaded PV module with the same PV module without shading in Fig. 7. The red dots in Fig. 7 show the MPPs. The maximum output power of the partially shaded PV module is about 56% of that of the same PV module without shading. As a result, one shaded PV cell degrades the PV module output power by as much as 44%, which establishes the significance of the partial shading effect.

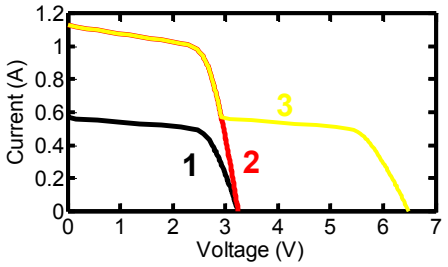

Fig. 6. The V-I output characteristics of the partially shaded PV module and its PV groups.

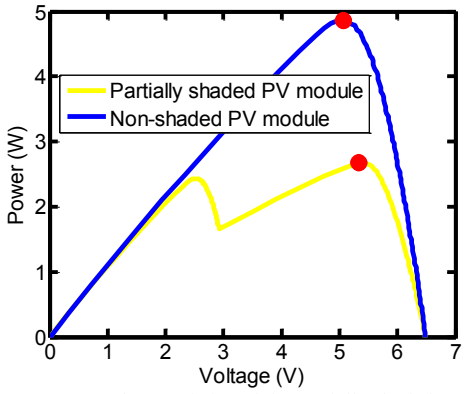

Fig. 7. The V-P output characteristics of the partially shaded PV module and the lighted PV module.

Partial shading may be caused by moving clouds, nearby buildings, trees, etc. It may also result from fallen leaves or dust on the PV modules [25], or other aging effects of PV modules [26]. In the former case, the partial shading pattern may be quite regular (i.e., like a block), and we call this case *block shading*. In the latter case, the partial shading pattern may be randomized, and we call this case *random shading*.

IV. PV Module Reconfiguration Architecture

We replace the conventional PV modules (with fixed configurations) by the reconfigurable PV modules for the PV system to combat partial shading. We make the *physical layout* and the *configuration* of a PV module independent of one another. The physical layout of the PV module is an $n' \times m'$ array on a panel, where there are n' rows and m' columns of PV cells. The configuration of the PV module is the actual electrical connection of PV cells in the PV module. We change the configuration of the PV module to counter partial shading. We introduce a reconfigurable PV module architecture as shown in Fig. 8. Each PV cell except for the last one is integrated with three switches i.e., a top P-switch $S_{PT,i}$, a bottom P-switch $S_{PB,i}$ and a S-switch $S_{S,i}$. The PV module reconfiguration is realized by controlling the ON/OFF states of these switches. The two P-switches of a PV cell are always in the same state, whereas its S-switch must be in the opposite state of the P-switches. The P-switches connect PV cells in parallel to form a PV group, while the S-switches connect the PV groups in series.

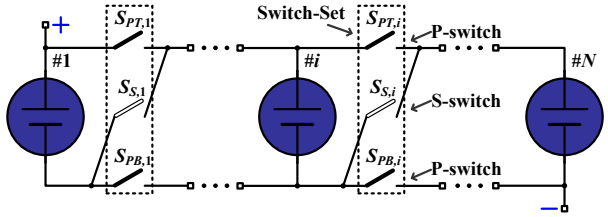

Fig. 8. The reconfigurable PV module architecture.

Fig. 9 is an example of PV module reconfiguration. The first four PV cells are connected in parallel to form PV Group 1; the next three PV cells form PV Group 2; and the last five PV cells form PV Group 3. These three PV groups are series-connected by the S-switches of the fourth and the seventh PV cells.

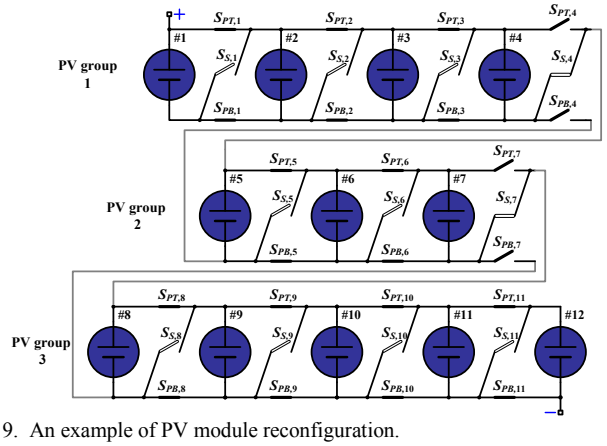

Fig. 9. An example of PV module reconfiguration.

A reconfigurable PV module consisting of N PV cells may include an arbitrary number (less than or equal to N) of PV

groups. The number of parallel-connected PV cells $r_j(>0)$ in the j-th PV group should satisfy

$$\sum_{j=1}^{g} r_j = N, \tag{7}$$

where g is the number of PV groups. We denote such a configuration by $\mathcal{C}(g;\, r_1, r_2, \cdots, r_g)$. This configuration can be viewed as a partition of the PV cell index set $\boldsymbol{A} = \{1, 2, 3, \cdots, N\}$, where the elements in $\boldsymbol{A}$ denote the indices of PV cells in the PV module. The partition is denoted by subsets $\boldsymbol{B}_1$, $\boldsymbol{B}_2$, ⋯, and $\boldsymbol{B}_g$ of $\boldsymbol{A}$, which correspond to the g PV groups consisting of r_1, r_2, ⋯, and r_g PV cells, respectively. The subsets $\boldsymbol{B}_1$, $\boldsymbol{B}_2$, ⋯, and $\boldsymbol{B}_g$ satisfy

$$\cup_{j=1}^{g} \boldsymbol{B}_j = \boldsymbol{A}, \tag{8}$$

and

$$\boldsymbol{B}_j \cap \boldsymbol{B}_k = \emptyset, \text{ for } \forall\, j, k \in \{1, 2, \cdots, g\} \text{ and } j \neq k. \tag{9}$$

The indices of PV cells in PV group j must be smaller than the indices of PV cells in PV group k for any $1 \le j < k \le g$ due to the structural characteristics of the reconfiguration architecture i.e., $i_1 < i_2$ for $\forall\, i_1 \in \boldsymbol{B}_j$ and $\forall\, i_2 \in \boldsymbol{B}_k$ satisfying $1 \le j < k \le g$. A partitioning satisfying the above properties is called an *alphabetical partitioning*.

V. Problem Formulation

Fig. 10 shows the architecture of a PV system. It contains M series-connected reconfigurable PV modules, each of which has the reconfiguration architecture shown in Fig. 8. The input and output ports of the charger are connected to the PV string and a supercapacitor array, respectively. The charger regulates the operation of the PV string by regulating its output voltage. The output current of the PV string is automatically determined based on its V-I characteristics. We adopt a software-based MPTT technique in the proposed PV system. It employs the perturb & observe (P&O) algorithm to maximize the charger output current through regulating the output voltage of PV string. For readers' convenience, notation used in the rest of this paper is summarized in Table I.

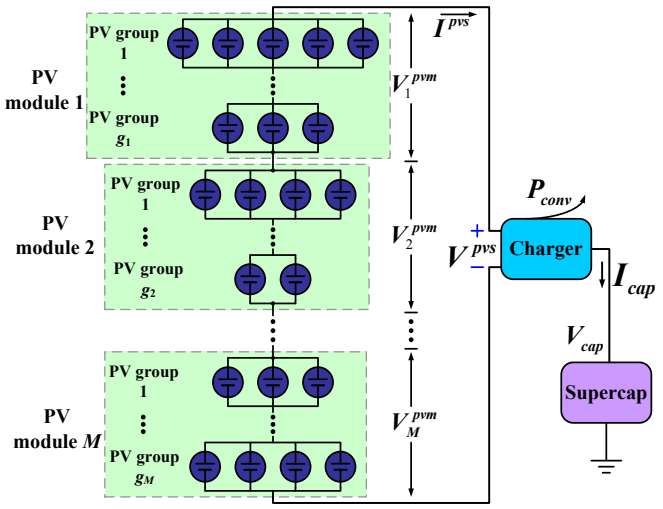

Fig. 10. The architecture of the PV system with reconfigurable PV modules.

TABLE I
Notations and Definitions

Symbol	Definition
$V_{k,i}^{pvc}, I_{k,i}^{pvc}$	Output voltage and current of the i-th PV cell in the k-th PV module
$G_{k,i}$	Solar irradiance level on the i-th PV cell of the k-th PV module
V_k^{pvm}, I_k^{pvm}	Output voltage and current of the k-th PV module
V^{pvs}, I^{pvs}	Output voltage and current of the PV string
M	Number of PV modules in the PV system
N	Number of PV cells in a PV module
P_{conv}	Power loss of the charger
V_{cap}	Terminal voltage of the supercapacitor array
I_{cap}	Input current of the supercapacitor array
g_k	Number of PV groups in the k-th PV module
$V_{k,j}^{pvg}, I_{k,j}^{pvg}$	Voltage and current of the j-th PV group of the k-th PV module
$r_{k,j}$	Number of PV cells in the j-th PV group of the k-th PV module
$\mathcal{C}_k(g_k;\, r_{k,1}, \cdots, r_{k,g_k})$	Configuration of the k-th PV module
$\boldsymbol{A} = \{1, 2, 3, \cdots, N\}$	PV cell index set
$\boldsymbol{B}_{k.1}, \boldsymbol{B}_{k,2}, \cdots, \boldsymbol{B}_{k,g_k}$	g_k subsets of $\boldsymbol{A}$ corresponding to configuration $\mathcal{C}_k(g_k;\, r_{k,1}, \cdots, r_{k,g_k})$
V_{avg}^{MPP}	Approximate PV cell MPP voltage
$I_{k,i}^{pvc,MPP}$	MPP current of the i-th PV cell in the k-th PV module
$V_{k,\mathrm{IC}}^{pvm,MPP}, I_{k,\mathrm{IC}}^{pvm,MPP}$	MPP voltage and current of the k-th ideal PV module
$\boldsymbol{\mathcal{C}}_{1\sim k}$	Configuration of the k-substring
$V_{1\sim k,\mathrm{IC}}^{pvs,MPP}, I_{1\sim k,\mathrm{IC}}^{pvs,MPP}$	MPP voltage and current of the ideal k-substring
$P_{1\sim k,\mathrm{IC}}^{pvs,MPP}$	MPP power of the ideal k-substring
$\boldsymbol{PO}_k$	Pareto-optimal set of the k-th PV module
$\boldsymbol{PO}_{1\sim k}$	Pareto-optimal configuration set of the k-substring

For the i-th PV cell in the k-th PV module, the relationship between $V_{k,i}^{pvc}$ and $I_{k,i}^{pvc}$ depends on $G_{k,i}$ as given by (1). Fig. 2 illustrates the V-I curves of a PV cell under different irradiance levels. We obtain $G_{k,i}$ of each PV cell using on-board solar irradiance sensors. The PV cell temperature has a relatively minor effect on the V-I characteristics. We derive the V-I curve of the k-th PV module given $\mathcal{C}_k(g_k;\, r_{k,1}, \cdots, r_{k,g_k})$. The output current of the k-th PV module is equal to the output current of any PV group in this PV module, i.e.,

$$I_k^{pvm} = I_{k,j}^{pvg} = \sum_{i \in \boldsymbol{B}_{k,j}} I_{k,i}^{pvc}, \forall\, j \in \{1, 2, \cdots g_k\}. \tag{10}$$

The output voltage of the k-th PV module is equal to the sum of the output voltages of its PV groups, i.e.,

$$V_k^{pvm} = \sum_{j=1}^{g_k} V_{k,j}^{pvg}, \tag{11}$$

where

$$V_{k,j}^{pvg} = V_{k,i}^{pvc}, \forall\, i \in \boldsymbol{B}_{k,j} \text{ and } j \in \{1, 2, \cdots g_k\}. \tag{12}$$

Similarly, the output current and voltage of the PV string satisfy the following:

$$I^{pvs} = I_k^{pvm}, \forall\, k \in \{1, 2, \cdots M\}, \tag{13}$$

and

$$V^{pvs} = \sum_{k=1}^{M} V_k^{pvm}. \tag{14}$$

The charger sets the operating point (V^{pvs}, I^{pvs}) of the PV string by controlling V^{pvs}, and I^{pvs} can be determined accordingly. Once the charger sets (V^{pvs}, I^{pvs}), the operating point of each PV cell is determined accordingly from (10) – (14). The charger power loss P_{conv} is determined by its input voltage, input current, output voltage, and output current, i.e., V^{pvs}, I^{pvs}, V_{cap}, and I_{cap}, respectively, from (5) and (6). According to (4), we have

$$V^{pvs} \cdot I^{pvs} = P_{conv} + V_{cap} \cdot I_{cap}. \quad (15)$$

where $I_{cap} = Chg\_Out\_I\left(V^{pvs}, I^{pvs}, V_{cap}\right)$.

We give a formal problem statement for the PV module reconfiguration (PMR) problem in the following.

PMR Problem Statement: Given $G_{k,i}$ of each i-th PV cell in the k-th PV module and V_{cap}, **find** the optimal $\mathcal{C}_k$ $(1 \le k \le M)$ of each PV module and the optimal (V^{pvs}, I^{pvs}), **such that** I_{cap} is maximized. The objective is equivalent to maximizing the PV system output power.

VI. PV Module Reconfiguration Control Algorithm

We define the output power at MPP of a PV cell/group/module/string by *MPP power*. The output power of the PV string and the output power of the PV system are positively correlated but they are different from one another because the former does not account for the charger power loss. We define the *MPP voltage* and *MPP current* of a PV cell/group/module/string as the output voltage and current of that PV cell/group/module/string at its MPP, respectively. The maximum solar power harvested by a PV system is the sum of the MPP power levels of all the PV cells in this system. The reconfiguration algorithm aims at making all PV cells to simultaneously operate at or close to their MPPs. We update the optimal configurations for PV modules according to the current shading pattern to maximize the PV system output power.

We make the following critical observations from the PV cell V-I and V-P characteristics shown in Fig. 2.

Observation I: The MPP voltage levels of a PV cell are very close to each other even under different solar irradiance levels. On the other hand, the MPP current values vary significantly under different solar irradiance levels.

Observation I is mainly due to the following two facts: (i) the MPP voltage level of a PV cell is largely determined by its open-circuit voltage level. The latter is a nearly constant value corresponding to the bias of the PV cell junction [24]. On the other hand, the MPP current is largely determined by the cell's photo-generated current $I_L(G)$, which is linearly dependent on the solar irradiance G according to Eqn. (2). Please refer to [24] for details. Observation I has already been adopted in some MPPT methods to combat the partial shading effect [7].

Observation I enables us to use a constant voltage V_{avg}^{MPP} to approximate the MPP voltage for every PV cell. We propose the *ideal PV cell* model based on Observation I. The V-I characteristics of an ideal PV cell is a step function such that

$$I_{k,i}^{pvc} = \begin{cases} I_{k,i}^{pvc,MPP}, & \text{if } V_{k,i}^{pvc} \le V_{avg}^{MPP}, \\ 0, & \text{otherwise}, \end{cases} \quad (16)$$

where $I_{k,i}^{pvc,MPP}$ is the MPP current of the PV cell, which is calculated from $G_{k,i}$ using the PV cell model in Section II.A. The ideal PV cell is an efficient and accurate approximation of the real PV cell, and plays an important role in the reconfiguration algorithm design.

We know that the MPP voltage of PV cell is close to V_{avg}^{MPP} at different solar irradiance levels. In the configuration shown in Fig. 11, the PV cell MPP current values, which are calculated from solar irradiance levels on PV cells, are labeled beside the PV cells. The sum of PV cell MPP current values in every PV group is 0.7 A. All the PV cells simultaneously operate close to their own MPPs with the configuration $\mathcal{C}(3;4,3,5)$ as shown in Fig. 11, when we set the output voltage of this PV module to $3 \cdot V_{avg}^{MPP}$. The output power of the PV module is maximized in this case. Hence, we arrive at the following observation.

Observation II: The MPP current values of all PV groups should be close to each other in a PV module, while the MPP current values of all the PV modules should be close to each other in the PV string to maximize the PV string output power.

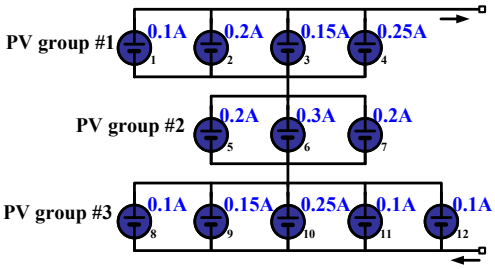

Fig. 11. An example of optimal PV module reconfiguration according to the PV cell MPP current values at their own MPPs.

The following Observation III is also important in determining the optimal PV module configurations:

Observation III: The charger power loss is minimized when the MPP voltage of the PV string and the supercapacitor terminal voltage are close to each other, according to the charger model described in Section II.B. In this case, the output power of the whole PV system can be further optimized.

A. Decomposing the Problem

We simplify the original PMR problem assuming *ideal PV cells* and name the new problem *Ideal PV Cell-based PMR* (IC-PMR) problem. Let $V_{k,\mathrm{IC}}^{pvm,MPP}(\mathcal{C}_k)$ and $I_{k,\mathrm{IC}}^{pvm,MPP}(\mathcal{C}_k)$ represent the MPP voltage and current values, respectively, of the k-th ideal PV module with a configuration $\mathcal{C}_k(g_k; r_{k,1}, \cdots, r_{k,g_k})$. Based on the ideal PV cell assumption, we calculate these values using the following identities:

$$V_{k,\mathrm{IC}}^{pvm,MPP}(\mathcal{C}_k) = g_k \cdot V_{avg}^{MPP}, \quad (17)$$

$$I_{k,\mathrm{IC}}^{pvm,MPP}(\mathcal{C}_k) = \min_{1 \le j \le g_k} \sum_{i \in \boldsymbol{B}_{k,j}} I_{k,i}^{pvc,MPP}, \quad (18)$$

Finally, the MPP voltage and current of the ideal PV string are given by $\sum_{k=1}^{M} V_{k,\mathrm{IC}}^{pvm,MPP}(\mathcal{C}_k)$ and $\min_{1 \le k \le M} I_{k,\mathrm{IC}}^{pvm,MPP}(\mathcal{C}_k)$, respectively. We have the following observation on the IC-PMR problem:

Observation IV: In the IC-PMR problem, the MPP of the PV string is the same PV string operating point that maximizes the output power of the PV system.

The IC-PMR problem is equivalent to: **find** optimal $\mathcal{C}_k$ of each PV module **such that** the charger output current, given by $Chg\_Out\_I\left(\sum_{k=1}^{M} V_{k,\mathrm{IC}}^{pvm,MPP}(\mathcal{C}_k), \min_{1\le k\le M} I_{k,\mathrm{IC}}^{pvm,MPP}(\mathcal{C}_k), V_{cap}\right)$, is maximized. From Observation IV, we do not need to separately find the optimal PV string operating point because it is exactly the MPP of the ideal PV string.

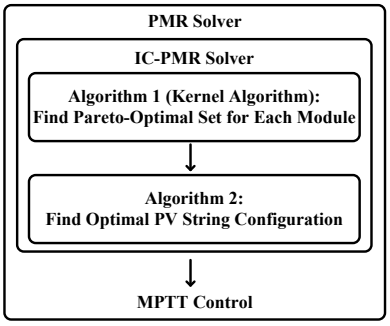

Fig. 12. The near-optimal solution of the PMR problem.

We propose a near-optimal solution of the original PMR problem in two steps: (i) PV module reconfiguration: optimally solving the IC-PMR problem and finding the corresponding optimal $\mathcal{C}_k$ for $1 \le k \le M$, based on the solar irradiance levels and V_{cap}, and (ii) MPTT: finding the optimal PV string operating point (V^{pvs}, I^{pvs}) that maximizes I_{cap} based on current V_{cap}. Fig. 12 illustrates the two steps in the proposed near-optimal solution. We introduce the optimal solution of the IC-PMR problem in the following.

B. Solution to the IC-PMR Problem

We propose to solve the IC-PMR problem in two steps as illustrated in Fig. 12. We first solve the problem of finding the optimal $\mathcal{C}_k(g_k; r_{k,1}, \cdots, r_{k,g_k})$ of each ideal PV module for each given $g_k \le N$, such that $P_{k,\mathrm{IC}}^{pvm,MPP}(\mathcal{C}_k)$ (or equivalently, $I_{k,\mathrm{IC}}^{pvm,MPP}(\mathcal{C}_k)$) is maximized. The solution to this problem is named the *kernel algorithm* and is based on dynamic programming. Let $\boldsymbol{PO}_k$ store all the optimal configurations of the k-th PV module with different g_k values. Next we find the optimal solution of the IC-PMR problem based on the optimization results of the kernel algorithm on every PV module. This step is based on the Pareto-optimal substructure property. We introduce these two steps one by one.

1) Step I: Kernel Algorithm

The kernel algorithm aims to maximize $I_{k,\mathrm{IC}}^{pvm,MPP}(\mathcal{C}_k)$ for given g_k. We name the problem the (N, g_k) *reconfiguration problem* to emphasize that g_k is given.

Consider a generalized problem that finds the optimal configuration for an l_1–cell ($l_1 \le N$, corresponding to the first l_1 cells of the original N cells in the k–th PV module) PV module composed of l_2 ($l_2 \le g_k$) PV groups, given $I_{k,i}^{pvc,MPP}$ ($1 \le i \le l_1$) and l_2. This is equivalent to finding the optimal alphabetical partitioning $\boldsymbol{B}_{k,1}^{l_1,l_2}, \boldsymbol{B}_{k,2}^{l_1,l_2}, \dots, \boldsymbol{B}_{k,l_2}^{l_1,l_2}$ of the set $\boldsymbol{A}^{l_1} = \{1, 2, 3, \cdots, l_1\}$, which is optimal in the sense that $\min_{1\le j\le l_2} \sum_{i\in \boldsymbol{B}_{k,j}^{l_1,l_2}} I_{k,i}^{pvc,MPP}$ is maximized. We call this problem the (l_1, l_2) *reconfiguration problem*. When $l_1 = N$ and $l_2 = g_k$, the (l_1, l_2) reconfiguration problem becomes the original (N, g_k) reconfiguration problem of the k–th PV module. We find the optimal substructure property of the (l_1, l_2) reconfiguration problem as described below, ensuring the applicability of dynamic programming.

Observation V *(The optimal substructure property):* Suppose that in the optimal solution of the (l_1, l_2) reconfiguration problem, the last (i.e., the l_2-th) PV group consists of $r_{k,l_2}^{l_1,l_2}$ PV cells. Consider the subproblem that finds the optimal configuration for the first $l_1 - r_{k,l_2}^{l_1,l_2}$ PV cells within $l_2 - 1$ PV groups. This corresponds to the $(l_1 - r_{k,l_2}^{l_1,l_2}, l_2 - 1)$ reconfiguration problem. The optimal solution of the (l_1, l_2) reconfiguration problem thus contains within it the optimal solution of the $(l_1 - r_{k,l_2}^{l_1,l_2}, l_2 - 1)$ reconfiguration problem.

Algorithm 1: The kernel algorithm.

Input: the number of PV cells N, the number of PV groups g_k, MPP current of each i-th ($1 \le i \le N$) PV cell $I_{k,i}^{pvc,MPP}$ (derived from $G_{k,i}$)

Output: the optimal PV module configuration $\mathcal{C}_k$.

Maintain two $N \times g_k$ matrices **Min_Sum_Opt** and **Last_Par**.

Initialize $\mathbf{Min\_Sum\_Opt}(l_1, 1) \leftarrow \sum_{1\le i\le l_1} I_{k,i}^{pvc,MPP}$.

Initialize $\mathbf{Last\_Par}(l_1, 1) \leftarrow 0$.

For l_2 from 2 to g_k:

  For l_1 from l_2 to N:

    $\mathbf{Min\_Sum\_Opt}(l_1, l_2) \leftarrow$

    $\max_{l_2-1\le l<l_1} \min\left\{\mathbf{Min\_Sum\_Opt}(l, l_2 - 1), \sum_{l<i\le l_1} I_{k,i}^{pvc,MPP}\right\}$

    $\mathbf{Last\_Par}(l_1, l_2) \leftarrow$

    $\operatorname{argmax}_{l_2-1\le l<l_1} \min\left\{\mathbf{Min\_Sum\_Opt}(l, l_2 - 1), \sum_{l<i\le l_1} I_{k,i}^{pvc,MPP}\right\}$

  End

End

Trace back using the matrix **Last_Par** to find the optimal $\mathcal{C}_k$ of the k-th PV module.

We have Algorithm 1 from the optimal substructure property as the kernel algorithm for solving the (N, g_k) reconfiguration problem with a given g_k. The time complexity of Algorithm 1 is $O(g_k \cdot N^2)$ (because we can pre-compute and store $\sum_{l<i\le l_1} I_{k,i}^{pvc,MPP}$ values in a matrix.) We make the size of matrices **Min_Sum_Opt** and **Last_Par** equal to $N \times N$ in order to solve the (N, g_k) reconfiguration problems for all $g_k \le N$ in one execution of Algorithm 1, with a total computation complexity of $O(N^3)$.

2) Step II: Optimal Solution of the IC-PMR Problem

We define the k-*substring* as the string consisting of PV modules 1, 2, …, k. The whole PV string is the M-substring. The configuration of the k-substring, $\boldsymbol{\mathcal{C}}_{1\sim k} = (\mathcal{C}_1, \mathcal{C}_2, \dots, \mathcal{C}_k)$, is a collection of the configurations of the 1st, 2nd, …, k-th PV modules. The MPP voltage and current of the ideal k-substring are $V_{1\sim k,\mathrm{IC}}^{pvs,MPP}(\boldsymbol{\mathcal{C}}_{1\sim k}) = \sum_{k'=1}^{k} V_{k',\mathrm{IC}}^{pvm,MPP}(\mathcal{C}_{k'})$ and $I_{1\sim k,\mathrm{IC}}^{pvs,MPP}(\boldsymbol{\mathcal{C}}_{1\sim k}) = \min_{1\le k'\le k} I_{k',\mathrm{IC}}^{pvm,MPP}(\mathcal{C}_{k'})$, respectively.

We define the Pareto-optimality and Pareto-optimal set of

the k-substring configurations.

Definition I *(Pareto superiority)**:*** Consider two configurations $\boldsymbol{\mathcal{C}}_{1\sim k}$ and $\widehat{\boldsymbol{\mathcal{C}}}_{1\sim k}$. $\boldsymbol{\mathcal{C}}_{1\sim k}$ is Pareto-superior to $\widehat{\boldsymbol{\mathcal{C}}}_{1\sim k}$ if $V_{1\sim k,\mathrm{IC}}^{pvs,MPP}(\boldsymbol{\mathcal{C}}_{1\sim k}) > V_{1\sim k,\mathrm{IC}}^{pvs,MPP}(\widehat{\boldsymbol{\mathcal{C}}}_{1\sim k})$ and $I_{1\sim k,\mathrm{IC}}^{pvs,MPP}(\boldsymbol{\mathcal{C}}_{1\sim k}) \geq I_{1\sim k,\mathrm{IC}}^{pvs,MPP}(\widehat{\boldsymbol{\mathcal{C}}}_{1\sim k})$, or $V_{1\sim k,\mathrm{IC}}^{pvs,MPP}(\boldsymbol{\mathcal{C}}_{1\sim k}) \geq V_{1\sim k,\mathrm{IC}}^{pvs,MPP}(\widehat{\boldsymbol{\mathcal{C}}}_{1\sim k})$ and $I_{1\sim k,\mathrm{IC}}^{pvs,MPP}(\boldsymbol{\mathcal{C}}_{1\sim k}) > I_{1\sim k,\mathrm{IC}}^{pvs,MPP}(\widehat{\boldsymbol{\mathcal{C}}}_{1\sim k})$.

Definition II *(Pareto-optimal configuration and Pareto-optimal set)**:*** $\boldsymbol{\mathcal{C}}_{1\sim k}$ is a *Pareto-optimal configuration* of the k-substring if no other configuration of the k-substring is Pareto-superior to it. The *Pareto-optimal* (*configuration*) *set* of the k-substring is represented by $\boldsymbol{PO}_{1\sim k}$.

We generalize the definition of Pareto-optimality and Pareto-optimal set to PV modules. The set $\boldsymbol{PO}_k$ obtained from the kernel algorithm is essentially the Pareto-optimal configuration set of the k-th PV module.

Theorem I demonstrates that finding the Pareto-optimal set $\boldsymbol{PO}_{1\sim M}$ of the M-substring, i.e., the whole PV string, will help in solving the IC-PMR problem. We rewrite the objective of the IC-PMR problem in Theorem I as finding the optimal $\boldsymbol{\mathcal{C}}_{1\sim M}$, which is equivalent to the original objective of finding optimal $\mathcal{C}_k$ for each PV module. Please see Appendix for the proof.

Theorem I *(Optimal configuration and Pareto-optimal configurations)**:*** The optimal $\boldsymbol{\mathcal{C}}_{1\sim M}$ that optimizes the IC-PMR problem is an element in $\boldsymbol{PO}_{1\sim M}$.

Consider the problem of finding $\boldsymbol{PO}_{1\sim M}$. We find the Pareto-optimal substructure property of this problem as shown in Theorem II. The proof of Theorem II is similar to that of Theorem I, and hence we omit the details of the proof.

Theorem II *(The Pareto-optimal substructure property)**:*** Suppose that $\boldsymbol{\mathcal{C}}_{1\sim k} = \{\mathcal{C}_1, \mathcal{C}_2, \dots, \mathcal{C}_{k-1}, \mathcal{C}_k\}$ is a Pareto-optimal configuration of the k-substring. Then $\{\mathcal{C}_1, \mathcal{C}_2, \dots, \mathcal{C}_{k-1}\}$ must be a Pareto-optimal configuration of the $(k-1)$-substring.

We propose Algorithm 2 that derives $\boldsymbol{PO}_{1\sim k}$ from $\boldsymbol{PO}_{1\sim(k-1)}$ based on the Pareto-optimal substructure property. We execute Algorithm 2 iteratively and find $\boldsymbol{PO}_{1\sim M}$ starting from $\boldsymbol{PO}_{1\sim 1} = \boldsymbol{PO}_1$, which is obtained from kernel algorithm.

Algorithm 2: Calculation of $\boldsymbol{PO}_{1\sim k}$.

Input: the Pareto-optimal configuration sets $\boldsymbol{PO}_{1\sim(k-1)}$ and $\boldsymbol{PO}_k$.

Output: the Pareto-optimal configuration set $\boldsymbol{PO}_{1\sim k}$.

Initialize $\boldsymbol{PO}_{1\sim k} \leftarrow \emptyset$.

For each $\boldsymbol{\mathcal{C}}_{1\sim(k-1)} = \{\mathcal{C}_1, \mathcal{C}_2, \dots, \mathcal{C}_{k-1}\} \in \boldsymbol{PO}_{1\sim(k-1)}$:

  For each $\mathcal{C}_k \in \boldsymbol{PO}_k$:

    $\boldsymbol{\mathcal{C}}_{1\sim k} \leftarrow \{\mathcal{C}_1, \mathcal{C}_2, \dots, \mathcal{C}_{k-1}, \mathcal{C}_k\}$.

    $\boldsymbol{PO}_{1\sim k} \leftarrow \boldsymbol{PO}_{1\sim k} \cup \boldsymbol{\mathcal{C}}_{1\sim k}$.

    Calculate $V_{1\sim k,\mathrm{IC}}^{pvs,MPP}(\boldsymbol{\mathcal{C}}_{1\sim k})$ and $I_{1\sim k,\mathrm{IC}}^{pvs,MPP}(\boldsymbol{\mathcal{C}}_{1\sim k})$ via:

$$V_{1\sim k,\mathrm{IC}}^{pvs,MPP}(\boldsymbol{\mathcal{C}}_{1\sim k}) = V_{1\sim(k-1),\mathrm{IC}}^{pvs,MPP}(\boldsymbol{\mathcal{C}}_{1\sim(k-1)}) + V_{k,\mathrm{IC}}^{pvm,MPP}(\mathcal{C}_k).$$

$$I_{1\sim k,\mathrm{IC}}^{pvs,MPP}(\boldsymbol{\mathcal{C}}_{1\sim k}) = \min\left\{I_{1\sim(k-1),\mathrm{IC}}^{pvs,MPP}(\boldsymbol{\mathcal{C}}_{1\sim(k-1)}), I_{k,\mathrm{IC}}^{pvm,MPP}(\mathcal{C}_k)\right\}.$$

  End

End

Remove all configurations from $\boldsymbol{PO}_{1\sim k}$ that are not Pareto-optimal.

The MPP voltage of an ideal PV module can only take N discrete values V_{avg}^{MPP}, $2 \cdot V_{avg}^{MPP}$, ..., $N \cdot V_{avg}^{MPP}$. Therefore, $\boldsymbol{PO}_k$ contains at most N different Pareto-optimal configurations while $\boldsymbol{PO}_{1\sim k}$ contains at most $k \cdot N$ different Pareto-optimal configurations. We implement Algorithm 2 with time complexity $k \cdot N^2$ making use of this property.

The last step in the IC-PMR solution is finding the optimal $\boldsymbol{\mathcal{C}}_{1\sim M}$ from $\boldsymbol{PO}_{1\sim M}$ that maximizes the charger output current, $Chg\_Out\_I\left(\sum_{k=1}^{M} V_{k,\mathrm{IC}}^{pvm,MPP}(\mathcal{C}_k), \min_{1\leq k\leq M} I_{k,\mathrm{IC}}^{pvm,MPP}(\mathcal{C}_k), V_{cap}\right)$. We summarize the steps of finding the optimal solution to the IC-PMR problem in Algorithm 3.

Algorithm 3: Summary of the optimal solution to the IC-PMR problem.

Input: the solar irradiance levels $G_{k,i}$ of each PV cell, supercapacitor voltage V_{cap}.

Output: the optimal configuration $\boldsymbol{\mathcal{C}}_{1\sim M}$.

Derive the MPP current of each PV cell, i.e., the $I_{k,i}^{pvc,MPP}$ values.

Run Algorithm 1 to calculate $\boldsymbol{PO}_k$ for every k-th ($1 \leq k \leq M$) PV module.

Run Algorithm 2 iteratively to calculate $\boldsymbol{PO}_{1\sim M}$ starting from $\boldsymbol{PO}_{1\sim 1} = \boldsymbol{PO}_1$.

Find the optimal configuration $\boldsymbol{\mathcal{C}}_{1\sim M}$ from $\boldsymbol{PO}_{1\sim M}$ that maximizes $Chg\_Out\_I\left(\sum_{k=1}^{M} V_{k,\mathrm{IC}}^{pvm,MPP}(\mathcal{C}_k), \min_{1\leq k\leq M} I_{k,\mathrm{IC}}^{pvm,MPP}(\mathcal{C}_k), V_{cap}\right)$.

C. Complexity, Overhead, and Implementation Details

The overall complexity of Algorithm 3 is $O(M \cdot N^3)$, or $O(\max(g_k) \cdot M \cdot N^2)$ if there is a constraint on the maximum number of groups (g_k values). For a relatively large-scale PV system with $M = 3$ and $N = 60$, it takes only 10 ms to calculate the optimal configuration on a 3.0 GHz desktop computer and should take less than 30 ms on a typical ARM-based embedded processor [27]. Moreover, since the switching time of MOSFET switches and regulation time of chargers are in the order of μs [28], performing reconfiguration and MPTT regulation are faster than computing the optimal configuration and have negligible time overhead.

The hardware overhead of the reconfiguration architecture will be mainly the additional switches. For example, the MOSFET switch in [31], which allows 10.3 A ON-current, costs only \$0.09. This is much cheaper than PV cells, which is above \$ 2 - 5/W. Besides, for larger-scale PV systems, the PV cell power rating can be much larger than 1 W.

Theoretically, if we want to maximize the energy accumulation over a time period with changing shading patterns and solar irradiance, we need to maximize the PV system output current at every time t in this period. In practice, we discretize the whole operating time of the PV system into a set of decision periods. At the beginning of each decision period, we obtain irradiance $G_{k,i}$ of each PV cell in the system using on-board solar irradiance sensors and the supercapacitor terminal voltage V_{cap}. We execute Algorithm 3 and find the optimal configuration of each PV module. We perform reconfiguration according to the derived configurations, and keep the configurations unchanged until next decision period.

The MPTT control is performed much more frequently to keep tracking the optimal operating point of the PV string.

The length of decision period depends on the shading types and applications. If the PV system is for vehicular usage, the decision period needs to be set small. If the shading is caused by a nearby building, the decision period can be longer. Since the overhead of reconfiguration algorithm is less than 30 ms, the decision period can be set much less than one second, which may be suitable for even fast shading applications.

VII. Experimental Results

A. Prototype of the PV Module with Reconfiguration

We implement a prototype of PV module reconfiguration to substantiate the feasibility and effectiveness of the proposed reconfiguration structure design and control algorithm. Fig. 13 shows the prototype of the reconfigurable PV module. The PV module consists of 16 PV cells. Each PV cell has a maximum output power of 1.2 W when the solar irradiance is 1000 W/m^2 under the standard test condition. We implement the reconfiguration network with a SPDT (single pole, double throw) switch as an S-switch and a DPDT (double pole, double throw) switch as a P-switch for each PV cell, because the two P-switches of a PV cell are always turned ON and OFF together. We mount the PV cells and toggle switches on top of an acrylic board, and route the connection wires in the back of the board. We operate the toggle switches manually in the prototype PV module. However, automatic switch control is not of high cost. We confirm the implementation of a computer-controlled programmable switch set using power MOSFETs and isolated gate drivers as shown in Fig. 14.

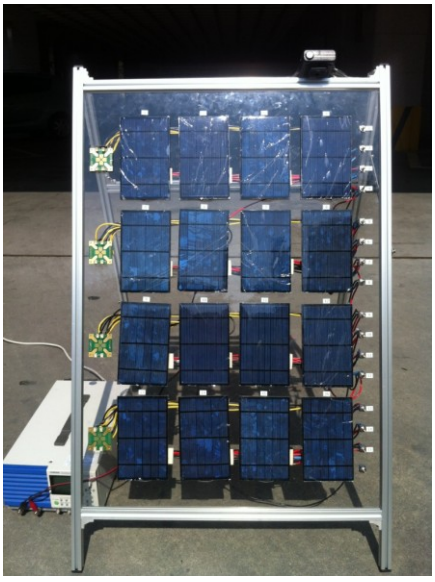

Fig. 13. The prototype PV module with reconfiguration.

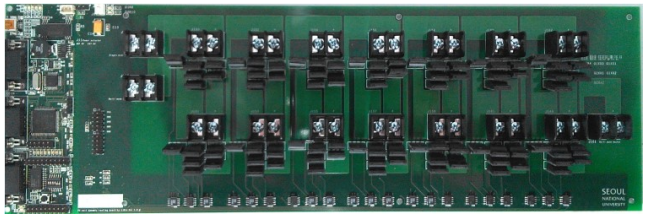

Fig. 14. The computer-controlled programmable switch board.

We measure the V-I characteristics and MPP values of a single PV cell in the reconfigurable PV module when the solar irradiance levels are 500 W/m^2, 770 W/m^2, and 1000 W/m^2, and temperature is 25 ℃. The measured V-I characteristics are shown in Fig. 15. Based on the measured V-I characteristics, we extract the unknown parameters $I_L(G_{STC})$, $I_0(T_{STC})$, R_s, R_p, and A of the PV cell model discussed in Section II.A, using the method proposed in [19]. The V-I characteristics of the PV simulation model are also shown in Fig. 15 after parameter extraction. The V-I curves of the measured PV cell and the simulation model match with each other in the entire operation range at all three solar irradiance levels, demonstrating the accuracy of the extracted PV cell simulation model.

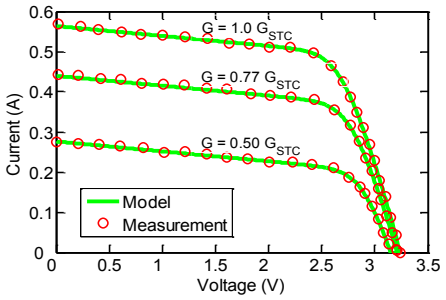

Fig. 15. Matching between the measurement results and the simulation model on the V-I characteristics of a single PV cell.

We demonstrate using the prototype the effectiveness of PV module reconfiguration to combat partial shading. We use paperboards to shade the corresponding PV cells in the PV module to implement the case of partial shading. We use the PV module to directly drive a controllable active load and measure the whole V-I and V-P curves of the PV module before and after reconfiguration. Then we derive the improvement of MPP using reconfiguration from the measured V-P characteristics. We test nine partial shading patterns, which contain one to ten completely shaded PV cells, as shown in Fig. 16.

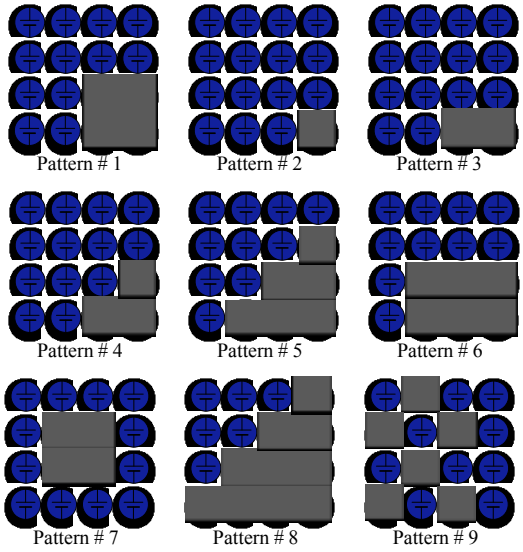

Fig. 16. Different partial shading patterns.

In the first shading pattern in Fig. 16, we shade four PV cells at the bottom right corner of the PV module. Then we optimally reconfigure the PV module into a $\mathcal{C}(3;4,4,8)$ configuration to maximize the output power. We measure the output power of

the PV module and confirm 36.3% output power level enhancement from reconfiguration compared with the original 4×4 configuration. Fig. 17 illustrates the measured V-P curves of the partially shaded PV module before and after reconfiguration, where the MPPs are marked by red dots. We can clearly see the improvement of the MPP of the partially-shaded PV module using the reconfiguration method. We also perform software simulation of the PV module and observe 36.1% output power level enhancement from reconfiguration against partial shading. This shows that the software simulation model is accurate.

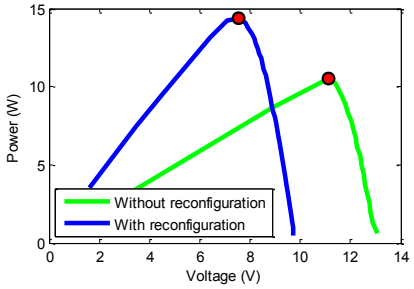

Fig. 17. Measured V-P curves of the partially shaded PV module (from the prototype) before and after reconfiguration.

Table II provides the MPP output power of the PV module before and after reconfiguration under all the nine partial shading patterns. It provides both measurement and simulation results. From the measurement results, we can observe that an improvement of 1.62 W to 3.90 W, or equivalent, 14.8% to 45.2%, can be achieved from the reconfiguration technique.

TABLE II
MPP OUTPUT POWER OF THE PV MODULE BEFORE AND AFTER RECONFIGURATION UNDER ALL THE NINE PARTIAL SHADING PATTERNS

Pattern	Power w/o recon		Power w/ recon		Improve
	Meas. (W)	Simu. (W)	Meas. (W)	Simu. (W)	Meas. (W/%)
#1	10.73	10.55	14.63	14.36	3.90 / 36.3%
#2	16.28	16.21	18.69	18.33	2.41 / 14.8%
#3	14.46	14.63	17.33	17.07	2.87 / 19.8%
#4	11.93	11.98	15.59	15.31	3.66 / 30.7%
#5	8.36	8.22	12.14	12.22	3.78 / 45.2%
#6	9.79	9.75	12.15	12.22	2.36 / 24.1%
#7	10.70	10.55	14.63	14.36	3.93 / 36.7%
#8	5.33	5.26	7.45	7.32	2.12 / 39.7%
#9	10.63	10.52	12.25	12.22	1.62 / 15.2%

B. Large-Scale PV System Simulations

We perform reconfiguration on large-scale PV modules and PV arrays using the simulation model. We ensure that the software simulation can present comparable results as those in the implementation due to the following three reasons: (i) We have derived accurate PV cell modeling from real measurements and it matches with real measurements at different solar irradiance levels. (ii) The V-I and V-P characteristics modeling of PV module and string is also accurate because they are essentially series and parallel connection of PV cells. In Section VII.A, we have already validated the output power improvement of the simulation model using real experiments on the PV module prototype. (iii) We have utilized accurate charger power model from [5], [20], which have been validated using HSPICE simulation.

We compare the performances of the PV system with reconfiguration and the baseline PV systems without reconfiguration. In the proposed PV system, we use reconfigurable PV modules with 60 PV cells in each module, a charger, and a 100 F supercapacitor as the energy storage. On the other hand, the PV modules in the baseline system have a fixed 10×6 configuration, where 10 PV groups are series-connected with 6 PV cells per PV group. We incorporate a software-based MPTT technique [16] in both the proposed PV system and the baseline system. In the baseline system, we incorporate bypass diodes for PV cells [11] to enhance the PV system output power and robustness under partial shading.

The first experiment considers a PV system with a single 60-cell PV module with the partial shading pattern shown in Fig. 18. We test the instantaneous output power level of the two PV systems. For the proposed system, Fig. 18 shows the physical locations of the PV cells in the PV module, instead of the actual electrical connection of the PV cells. Table III summarizes the output power improvement of the proposed PV system compared to the baseline system given the shading pattern and different V_{cap} values. As shown in Table III, the proposed PV system with reconfiguration achieves up to 42% output power improvement compared with the baseline system when $V_{cap} = 15$ V, thereby demonstrating the effectiveness of the reconfigurable method. Table III also shows (i) the actual PV system output power of the proposed system and baseline system, and (ii) the near-optimal PV module configuration obtained by the reconfiguration control algorithm.

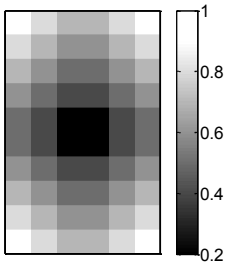

Fig. 18. Partial shading pattern of the single PV module in the 1st experiment.

TABLE III
IMPROVEMENT OF INSTANTANEOUS OUTPUT POWER OF THE PV SYSTEM IN THE FIRST EXPERIMENT

V_{cap} (V)	5	15	25
Output power improvement	1.39X	1.42X	1.40X
Output power Proposed/Baseline	31.01 W/ 22.32 W	38.40 W/ 27.04 W	37.75 W/ 26.93 W
PV module configuration	$\mathcal{C}$(2;30,30)	$\mathcal{C}$(7;6,7,10,14,10,7,6)	$\mathcal{C}$(7;6,7,10,14,10,7,6)

Two factors contribute to the PV system output power improvement. The first is the enhancement in the maximum output power of the PV module due to reconfiguration. Fig. 19 plots the V-P curves of the PV module in the two systems with the shading pattern in Fig. 18 and a V_{cap} value of 15 V. The proposed reconfigurable PV module achieves a peak output

power much higher than that of the baseline PV module. The second factor is the ability to achieve through reconfiguration a better match between the MPP voltage of the PV module and the terminal voltage of the supercapacitor. In this way, the charger consumes the least amount of power and the output power of the PV system can be maximized.

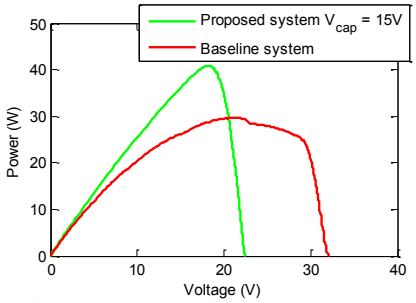

Fig. 19. V-P characteristics of the PV modules with and without reconfiguration technique.

In reality, temperatures of different PV cells in a system can be different due to the partial shading effect. We perform in-field measurement and confirm a maximum of 10 ℃ difference between temperature of the lighted PV cell and that of the shaded PV cell. 10 ℃ higher in temperature will result in $< 5\%$ degradation in the MPP voltage of PV cell according to the model presented in Section II.A and reference [32]. We perform experiments using the same PV system setup as shown in Fig. 18. For simplicity, we assume two levels of temperature in the PV system: 25 ℃ (same as before) for PV cells with solar irradiance less than $500\ \mathrm{W/m^2}$ ($0.5\ G_{STC}$), and 35 ℃ for the other PV cells with higher solar irradiance. Table IV summarizes the actual output power of the two systems and improvement of the proposed system. We can observe that although slight output power degradation can be observed when comparing with Table III, the relative improvement remains nearly the same. This is because the output power degradation due to higher temperature affects both proposed system and baseline system.

TABLE IV
IMPROVEMENT OF INSTANTANEOUS OUTPUT POWER OF THE PV SYSTEM IN THE FIRST EXPERIMENT CONSIDERING TEMPERATURE EFFECT

V_{cap} (V)	5	15	25
Output power improvement	1.39X	1.41X	1.39X
Output power Proposed/Baseline	30.24 W/ 21.80 W	36.89 W/ 26.18 W	35.78 W/ 25.75 W

The second experiment takes into account a PV system with three 60-cell PV modules with partial shading pattern shown in Fig. 20. We test the instantaneous output power level of the two PV systems. Table V summarizes the output power improvement of the proposed PV system compared to the baseline system, given the shading pattern and the V_{cap} value. It also provides the near-optimal PV module configuration obtained by the reconfiguration control algorithm. The proposed reconfigurable PV system achieves up to 76% output power enhancement compared with the baseline system, which shows that the proposed PV module reconfiguration technique achieves more benefits for the string charger architecture.

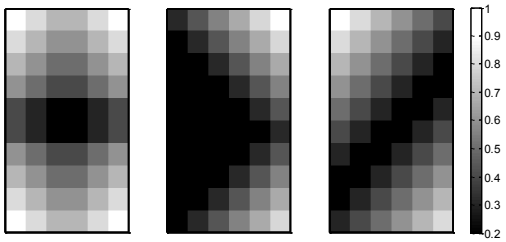

Fig. 20. Partial shading pattern of the three PV modules in the 2nd experiment.

TABLE V
IMPROVEMENT OF INSTANTANEOUS OUTPUT POWER OF THE PV SYSTEM IN THE SECOND EXPERIMENT

V_{cap} (V)	20	40	60
Output power improvement	1.58X	1.65X	1.76X
PV module #1 configuration	$\mathcal{C}$(9;5,5,6,7,14,7,6,5,5)	$\mathcal{C}$(11;4,4,5,5,6,12,6,5,5,4,4)	$\mathcal{C}$(11;4,4,5,5,6,12,6,5,5,4,4)
PV module #2 configuration	$\mathcal{C}$(5;8,9,17,18,8)	$\mathcal{C}$(6;6,9,9,18,11,7)	$\mathcal{C}$(6;6,9,9,18,11,7)
PV module #3 configuration	$\mathcal{C}$(7;5,6,8,12,15,8,6)	$\mathcal{C}$(8;4,5,6,10,14,9,7,5)	$\mathcal{C}$(8;4,5,6,10,14,9,7,5)

We investigate the maximum enhancement in PV system output power using reconfiguration. We consider a PV system with three 60-cell PV modules with partial shading pattern shown in Fig. 21. The proposed PV module reconfiguration technique achieves up to 2.36X output power enhancement under this partial shading pattern as shown in Table VI.

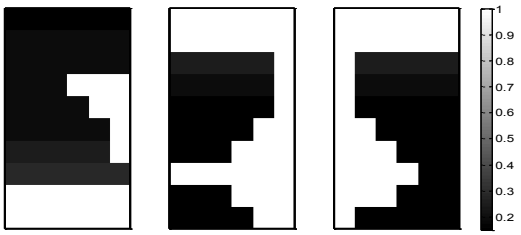

Fig. 21. Partial shading pattern of the three PV modules for maximum output power improvement.

TABLE VI
IMPROVEMENT OF INSTANTANEOUS OUTPUT POWER OF THE PV SYSTEM IN THE THIRD EXPERIMENT TO TEST THE MAXIMUM GAIN

V_{cap} (V)	20	50	80
Output power improvement	1.85X	2.01X	2.36X

Finally, we test the overall efficiency of the two PV systems in a time period of 30 minutes over random shading. We consider the following two test cases:

- 1/2 of the PV cells in the three PV modules are shaded, and the solar irradiance levels on these shaded PV cells are uniformly distributed within the range $[0.1G_{STC}, 0.5G_{STC}]$ and change with time.
- 2/3 of all the PV cells are shaded, and the solar irradiance levels on these PV cells are uniformly distributed within the range $[0.1G_{STC}, 0.5G_{STC}]$.

The proposed PV system updates its module configurations once per minute according to the current shading pattern and charger efficiency variation. We compare the electrical energy

stored into the supercapacitors in the two systems during this time period. The proposed PV system achieves 53% and 88% improvements compared to the baseline system in the two test cases, respectively.

VIII. CONCLUSION

This paper addresses the output power degradation problem of a PV system with the string charger interface under partial shading. The string charger interface is widely used and cost effective, but very vulnerable to partial shading effects. We introduce the PV module reconfiguration technique to combat the partial shading effects. As importantly, we provide an effective reconfiguration control algorithm, which realizes adaptive and near-optimal PV module reconfiguration for each PV module in the PV string according to the partial shading pattern and the conversion efficiency variation of the charger. The proposed reconfiguration control algorithm is based on dynamic programming with polynomial time complexity.

REFERENCES

[1] X. Lin, Y. Wang, S. Yue, D. Shin, N. Chang, and M. Pedram, "Near-optimal, dynamic module reconfiguration in a photovoltaic system to combat partial shading effects," in *Proc. 49th Annual Design Automation Conf. (DAC)*, San Francisco, 2012, pp. 516-521.

[2] N. Femia, G. Petrone, G. Spagnuolo, and M. Vitelli, "Optimization of perturb and observe maximum power point tracking method," *IEEE Trans. Power Electronics*, vol. 20, pp. 963-973, Jul. 2005.

[3] F. Liu, S. Duan, F. Liu, B. Liu, and Y. Kang, "A variable step size INC MPPT method for PV systems," *IEEE Trans. Industrial Electron.*, 2008.

[4] Y. Kim, N. Chang, Y. Wang, and M. Pedram, "Maximum power transfer tracking for a photovoltaic-supercapacitor energy system," in *Proc. 16th Int. Symposium Low Power Electronics and Design (ISLPED)*, 2010.

[5] Y. Wang, X. Lin, Y. Kim, N. Chang, and M. Pedram, "Enhancing efficiency and robustness of a photovoltaic power system under partial shading," in *Proc. Int. Symposium Quality of Electronic Design (ISQED)*, Santa Clara, 2012, pp. 592-600.

[6] C. Lu, V. Raghunathan, and K. Roy, "Maximum power point considerations in micro-scale solar energy harvesting systems," in *Proc. IEEE Int. Symposium Circuits and Systems (ISCAS)*, 2010.

[7] H. Patel, and V. Agarwal, "Maximum power point tracking scheme for PV systems operating under partially shaded conditions," *IEEE Trans. Industrial Electronics*, vol. 55, pp. 1689-1698, Apr. 2008.

[8] R. Bruendlinger, B. Bletterie, M. Milde, and H. Oldenkamp, "Maximum power point tracking performance under partially shaded PV array conditions," in *Proc. 21st EUPVSEC*, 2006, pp. 2157.

[9] T. L. Nguyen, and K. Low, "A global maximum power point tracking scheme employing DIRECT search algorithm for photovoltaic systems," *IEEE Trans. Industrial Electronics*, vol. 57, pp. 3456-3467, Oct. 2010.

[10] M. Miyatake, T. Inada, I. Hiratsuka, H. Zhao, H. Otsuka, and M. Nakano, "Control characteristics of a fibonacci-search-based maximum power point tracker when a photovoltaic array is partially shaded," in *Proc. Int. Power Electronics and Motion Control Conf. (IPEMC)*, 2004.

[11] D. Nguyen, and B. Lehman, "An adaptive solar photovoltaic array using model-based reconfiguration algorithm," *IEEE Trans. Industrial Electronics*, vol. 55, pp. 2644-2654, Jul. 2008.

[12] G. Velasco-Quesada et al, "Electrical PV array reconfiguration strategy for energy extraction improvement in grid-connected PV systems," *IEEE Trans. Industrial Electronics*, 2009.

[13] M. A. Chaaban et al, "Adaptive photovoltaic system," in *Proc. 36th Annual Conf. IEEE Industrial Electronics Society (IECON)*, 2010.

[14] R. Candela, V. D. Dio, E. R. Sanseverino, and P. Romano, "Reconfiguration techniques of partial shaded PV systems for the maximization of electrical energy production," in *Proc. Int. Conf. Clean Electrical Power (ICCEP)*, Capri, 2007, pp. 716-719.

[15] Y. Auttawaitkul, B. Pungsiri, K. Chammongthai, and M. Okuda, "A method of appropriate electrical array reconfiguration management for photovoltaic powered car," in *Proc. IEEE Asia-Pacific Conf. Circuits and Systems (IEEE APCCAS)*, Chiangmai, 1998, pp. 201-204.

[16] Y. Kim, S. Park, Y. Wang, Q. Xie, N. Chang, M. Poncino, and M. Pedram, "Balanced reconfiguration of storage banks in a hybrid electrical energy storage system," in *Proc. Int. Conf. Computer-Aided Design (ICCAD)*, San Jose, 2011, pp. 624-631.

[17] Y. Wang, X. Lin, N. Chang, and Massoud Pedram, "Dynamic reconfiguration of photovoltaic energy harvesting system in hybrid electric vehicles," in *Proc. 18th Int. Symposium Low Power Electronics and Design (ISLPED)*, Redondo Beach, CA, USA, 2012.

[18] X. Lin, Y. Wang, D. Zhu, N. Chang, and M. Pedram, "Online fault detection and tolerance for photovoltaic energy harvesting systems," in *Proc. Int. Conf. Computer-Aided Design (ICCAD)*, San Jose, 2012.

[19] W. Lee, Y. Kim, Y. Wang, N. Chang, M. Pedram, and S. Han, "Versatile high-fidelity photovoltaic module emulation system," in *Proc. 17th Int. Symposium Low Power Electronics and Design (ISLPED)*, 2011.

[20] Y. Choi, N. Chang, and T. Kim, "DC-DC converter-aware power management for low-power embedded systems," *IEEE Trans. CAD of Integrated Circuits and Systems (TCAD)*, 2007.

[21] Y. Wang, Y. Kim, Q. Xie, N. Chang, and M. Pedram, "Charge migration efficiency optimization in hybrid electrical energy storage (HEES) systems," in *Proc. 17th Int. Symposium Low Power Electronics and Design (ISLPED)*, Fukuoka, 2011, pp. 103-108.

[22] M. S. Swaleh, and M. A. Green, "Effect of shunt resistance and bypass diodes on the shadow tolerance of solar cell modules," *Solar Cells*, vol. 5, pp. 183-198, Jan. 1982.

[23] Linear Technology LTM4607: http://cds.linear.com/docs/en/datasheet/4607fb.pdf.

[24] GEOS24705 Solar Photovoltaics EJM May 2011 http://geosci.uchicago.edu/~moyer/GEOS24705/2011/Notes/SolarPhysics.pdf.

[25] S. A. Sulaiman, H. Hussain, N. Nik Leh, and M. S. I. Razali, "Effects of dust on the performance of PV panels," *World Academy of Science, Engineering and Technology*, 2011.

[26] Failure Modes of Crystalline Si Modules, http://www1.eere.energy.gov/solar/pdfs/pvrw2010_wohlgemuth_silicon.pdf.

[27] Samsung Exynos 4 Dual 45nm (Exynos 4210) RISC Microprocessor, 2012.

[28] S. Park, J. Park, D. Shin, Y. Wang, Q. Xie, M. Pedram, and N. Chang, "Accurate modeling of the delay and energy overhead of dynamic voltage and frequency scaling in modern microprocessors," in *IEEE Trans. on CAD of Integrated Circuits and Systems*, 2013.

[29] X. Jiang, J. Polastre, and D. Culler, "Perpetual environmentally powered sensor networks," *Proc. of International Symposium on Information Processing in Sensor Networks* (IPSN), 2005.

[30] S. J. Chiang, K. T. Chang, and C. Y. Yen, "Residential photovoltaic energy storage system," *IEEE Trans. on Industrial Electronics*, 1998.

[31] DMG4406LSS MOSFET, http://www.diodes.com/datasheets/DMG4406LSS.pdf.

[32] W. De Soto, S. A. Klein, and W. A. Beckman, "Improvement and validation of a model for photovoltaic array performance," *Solar Energy*, 2006.

APPENDIX: PROOF OF THEOREM I

We use proofs by contradiction. Suppose that the optimal $\boldsymbol{C}_{1\sim M}$ that optimizes the IC-PMR problem is NOT an element in $\boldsymbol{PO}_{1\sim M}$. Then there exists a configuration of the PV string, denoted by $\widehat{\boldsymbol{C}}_{1\sim k}$, that is Pareto-superior to $\boldsymbol{C}_{1\sim M}$, which implies that $V_{1\sim k,\mathrm{IC}}^{pvs,MPP}(\widehat{\boldsymbol{C}}_{1\sim k}) > V_{1\sim k,\mathrm{IC}}^{pvs,MPP}(\boldsymbol{C}_{1\sim k})$ and $I_{1\sim k,\mathrm{IC}}^{pvs,MPP}(\widehat{\boldsymbol{C}}_{1\sim k}) \geq I_{1\sim k,\mathrm{IC}}^{pvs,MPP}(\boldsymbol{C}_{1\sim k})$, or $V_{1\sim k,\mathrm{IC}}^{pvs,MPP}(\widehat{\boldsymbol{C}}_{1\sim k}) \geq V_{1\sim k,\mathrm{IC}}^{pvs,MPP}(\boldsymbol{C}_{1\sim k})$ and $I_{1\sim k,\mathrm{IC}}^{pvs,MPP}(\widehat{\boldsymbol{C}}_{1\sim k}) > I_{1\sim k,\mathrm{IC}}^{pvs,MPP}(\boldsymbol{C}_{1\sim k})$. Then according to the property of charger as described in Section II.B, the charger output current with PV string configuration $\widehat{\boldsymbol{C}}_{1\sim k}$, $Chg\_Out\_I\left(V_{1\sim k,\mathrm{IC}}^{pvs,MPP}(\widehat{\boldsymbol{C}}_{1\sim k}), I_{1\sim k,\mathrm{IC}}^{pvs,MPP}(\widehat{\boldsymbol{C}}_{1\sim k}), V_{cap}\right)$, is higher than the charger output current with PV string configuration $\boldsymbol{C}_{1\sim k}$, $Chg\_Out\_I\left(V_{1\sim k,\mathrm{IC}}^{pvs,MPP}(\boldsymbol{C}_{1\sim k}), I_{1\sim k,\mathrm{IC}}^{pvs,MPP}(\boldsymbol{C}_{1\sim k}), V_{cap}\right)$. This implies that $\boldsymbol{C}_{1\sim M}$ cannot optimize the IC-PMR problem.

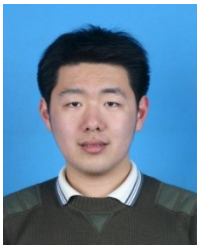

Yanzhi Wang (S'12) received the B.S. degree with distinction in electronic engineering from Tsinghua University, Beijing, China, in 2009. He is currently pursuing the Ph.D. degree in electrical engineering at University of Southern California, under supervision of Prof. Massoud Pedram. His current research interests include system-level power management, next-generation energy sources, hybrid electrical energy storage systems, near-threshold computing, cloud computing, mobile devices and smartphones, and the smart grid. He has published around 80 papers in these areas.

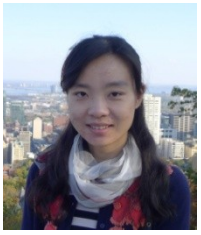

Xue Lin (S'12) received the B.S. degree from Tsinghua University, Beijing, China, in 2009. She is now a Ph.D. student in the Department of Electrical Engineering at University of Southern California. Her advisor is Prof. Massoud Pedram. She has been working on power management of photovoltaic (PV) systems, near-threshold computing of FinFET circuits, and power management of energy storage systems. She has published around 30 papers in these areas.

Younghyun Kim (M'13) received the B.S. degree (with the highest honor) in computer science and engineering and Ph.D. degree in electrical engineering and computer science from Seoul National University, Seoul, Korea, in 2007 and 2013, respectively. From 2009 to 2011, he was a Visiting Scholar with the University of Southern California, Los Angeles, CA, USA. He is currently a Postdoctoral Research Assistant at School of Electrical and Computer Engineering, Purdue University, West Lafayette, IN, USA. His current research interest includes secure medical devices, system-level power management, and energy harvesting and storage systems.

Dr. Kim was ISLPED Low Power Design Contest winner in 2007 and 2012, and received IEEE SSCS Seoul Chapter Best Paper Award in ISOCC 2009.

Naehyuck Chang (F'12) received the B.S., M.S., and Ph.D. degrees from the Department of Control and Instrumentation, Seoul National University, Seoul, Korea, in 1989, 1992, and 1996, respectively. He joined the Department of Computer Engineering, Seoul National University, in 1997, and is currently a Professor with Department of Electrical Engineering and Computer Science, Seoul National University, and the Vice Dean of College of Engineering, Seoul National University. His current research interests include low-power embedded systems, hybrid electrical energy storage systems, next-generation energy sources. He serves (and served) on the technical program committees in many EDA conferences, including DAC, ICCAD, ISLPED, DATE, CODES+ISSS, and ASP-DAC. He was a TPC (Co-)Chair of RTCSA 2007, ISLPED 2009, ESTIMedia 2009 and 2010, and CODES+ISSS 2012, and will serve as TPC Chair of ICCD 2013, General Chairs of ICCD 2014, VLSI-SoC 2015, and ASP-DAC 2015. He was the General Vice-Chair of ISLPED 2010, General Chair of ISLPED 2011 and ESTIMedia 2011. He is (was) an Associate Editor of IEEE TCAS-I, IEEE TCAD, ACM TODAES, and ACM TECS, Springer DAEM, IEEE Embedded Systems Letter, and was a Guest Editor of ACM TODAES in 2010, and ACM TECS in 2010 and 2011. He is the ACM SIGDA Chair and an ACM Distinguished Scientist.

Massoud Pedram (F'01), who is the Stephen and Etta Varra Professor in the Ming Hsieh department of Electrical Engineering at University of Southern California, received a Ph.D. in Electrical Engineering and Computer Sciences from the University of California, Berkeley in 1991. He holds 10 U.S. patents and has published four books, 12 book chapters, and more than 140 archival and 350 conference papers. His research ranges from low power electronics, energy-efficient processing, and cloud computing to photovoltaic cell power generation, energy storage, and power conversion, and from RT-level optimization of VLSI circuits to synthesis and physical design of quantum circuits. For this research, he and his students have received six conference and two IEEE Transactions Best Paper Awards. Dr. Pedram is a recipient of the 1996 Presidential Early Career Award for Scientists and Engineers, a Fellow of the IEEE, an ACM Distinguished Scientist, and currently serves as the Editor-in-Chief of the ACM Transactions on Design Automation of Electronic Systems. He has also served on the technical program committee of a number of premiere conferences in his field and was the founding Technical Program Co-chair of the 1996 International Symposium on Low Power Electronics and Design and the Technical Program Chair of the 2002 International Symposium on Physical Design.